Review: Real-space analyses of local dynamics in liquid using X-ray scattering[1]

Yuya Shinohara,[1] Takuya Iwashita,[2] Takeshi Egami[1,3]
[1]Materials Science and Technology Division, Oak Ridge National Laboratory, [2]Oita University,
[3]Department of Materials Science and Engineering, and Department of Physics and Astronomy, University of Tennessee, Knoxville

Abstract
In this review, we advocate describing the liquid dynamics using the Van Hove correlation function, a temporal and spatial correlation function. Recent progress in X-ray optics and X-ray sources makes it possible to carry out inelastic and quasi-elastic x-ray scattering whose spectra can be converted into the dynamic correlation function in real space. We describe the basic concept of the Van Hove correlation function, how it is obtained from the X-ray scattering spectra using synchrotron X-rays and X-ray free electron lasers, and the atomic dynamics in water and aqueous salt solution.

1. Introduction

A liquid is one of the fundamental states of matter. We learn this at elementary schools. Regardless, there are not many scientists who can discuss the physics of liquids compared to the other states of matter, gas and solid. Discussion on the specific heat of ideal gas and crystals at a molecular level is standard in statistical physics at undergraduate/graduate levels. However, not so many scientists have discussed the specific heat of liquid on a microscopic scale. Nowadays, in many colleges, a basic course of physics does not include fluid dynamics that describes the macroscopic behavior of fluids, including liquids. So, although it is daily material, the liquid is a subject such that even many professional physic scientists do not understand both the macroscopic and microscopic behavior.

One example that shows our incomplete understanding of liquid physics is the changes in viscosity in an aqueous salt solution. In an aqueous solution, the dependence of viscosity on the ion concentration is approximated by the following Jones–Dole equation [1,2]:

$$\frac{\eta}{\eta_w} = 1 + A\sqrt{c} + Bc + \cdots,$$

where η, η_w are the viscosity of aqueous solution and pure water, respectively, and c is the concentration of ions. The A-coefficient is explained by force between ions, but a reasonable explanation has not been given to B-coefficient. **Fig. 1** shows the B-coefficient at room temperature [1]. When the B-coefficient is positive, the viscosity increases as the ion concentration increases, while the viscosity decreases when the B-coefficient is negative. One of the explanations for this behavior is that ions enhance or destroy the hydrogen-bonded network depending on the types of ions, and ions are classified as either *structure maker* or *structure breaker* [3]. This argument ignores their dynamics, and such a description where the structural viewpoint is highlighted too much is inappropriate. Neutron scattering, X-ray scattering, and molecular dynamics (MD) simulation have provided information about the Pair Distribution Function (PDF) [4], which allows us to obtain the averaged structure of water molecules surrounding the ions [5]. However, the PDF analyses provide only the averaged *snapshot* of molecular configuration, and it is not sufficient to

[1] The original document which will be submitted and published is written in Japanese. This draft is a *direct* translation into English for review purposes.

discuss the physics of fluids, particularly their transport phenomena. Various optical spectroscopies have identified the intramolecular and rotational dynamics [6-9], but they do not contain their spatial information. Understanding of the local dynamics of water molecules surrounding ions is insufficient, and the effect of ions on the transport properties of the aqueous salt solution remains controversial. Understanding and controlling the transport properties of liquid at a microscopic scale is important for both basic research and the energy-related application such as butteries [10]. From the physiological point of view, the effect of ions on the transport properties of an aqueous solution needs to be elucidated to understand better the Hofmeister series that controls the salt-in and salt-out of proteins.

It is not trivial to set a starting point to discuss the dynamics of liquids [11]. In liquid, there is no long-range order as in crystals nor ideal disorder as in ideal gas. The diffusive motion of particles is not just a simple random walk but strongly correlated. When crystals are studied by X-ray and neutron scattering, elastic scattering provides the structural information, quasi-elastic scattering reflects the diffusion behavior, and inelastic scattering provides the lattice vibration (phonons). Their timescale and energy scale are different and can be discussed separately. In liquids, their timescale is similar, at picoseconds. Therefore, it is not trivial how to separate them experimentally, and we need to introduce a new framework to discuss the physics of liquids, not simply extrapolating the physics formulated for solids and gas.

Inelastic and quasi-elastic scattering of neutrons and X-rays have been used to measure the microscopic dynamics of liquids. When Q is small (e.g., $Q < 2$ nm^{-1} for water), hydrodynamic description of liquid is effective [12], and its microscopic phenomena such as sound speed have been studied. In many cases, the dynamic structure factor is described by the generalized Langevin equation using memory functions, and the experimental data have been analyzed by fitting the spectra in reciprocal and energy space. Description in reciprocal space is powerful when the system possesses a long-range order, there exists a hidden long-range order, or the system is described by the perturbation from the long-range order. Such assumptions do not apply to liquid and the description in real space is more appropriate than that in reciprocal space. We have thus introduced the temporal and spatial correlation function introduced by Van Hove [13] and have studied the local dynamics in liquid using this Van Hove correlation function [14-17]. Right after Van Hove showed the relationship between the correlation function and the scattering cross-section, Brockhouse reported the Van Hove correlation function of liquid lead by using inelastic neutron scattering [18]. In molecular dynamics simulation, the trajectory of all the particles can easily be recorded, the Van Hove correlation function can easily be studied, and its self-part has been used to discuss the particles' self-diffusive motion, which is one of the main topics in the textbooks of liquid physics [19-21]. In experiments, measuring the Van Hove correlation function of atoms and molecules is not straightforward as mentioned later. Thus, after the pioneering work by Brockhouse, the Van Hove function has hardly been measured experimentally except for a few tries [22].

As described in the following sections, the Van Hove correlation function is related, via Fourier transformation, to the dynamic structure factor that can be obtained from the inelastic scattering of X-rays or neutrons. Thus, if the data that can be used for the Fourier transformation, the Van Hove correlation function can be obtained. This requires the measurement of inelastic scattering spectra over wide energy transfer ($E= \hbar\omega$) and momentum transfer (Q) with a sufficient energy resolution and angular resolution within a reasonable time. Such a measurement has been realized thanks to the recent development in the highly brilliant X-rays and high-resolution spectrometer in X-ray scattering [23,24] and wide-Q measurement using pulsed neutron and time-of-flight measurement in neutron scattering. Recent progress in X-ray free electron laser and wide-Q measurement using wide-angle spin-echo spectrometer will broaden

the temporal and spatial range that can be accessed by the current approach. In this review article, we introduce the real-space analyses of liquid using inelastic X-ray scattering.

2. Van Hove Correlation Function

2.1. Definition

The Scattering cross-section that is measured by inelastic scattering of X-rays and neutron is related to the dynamic structure factor, $S(Q,E)$ [13]. By calculating its Fourier transform over an energy transfer, E, an intermediate scattering function, $F(Q,t)$, is given. Intermediate scattering function, $F(Q,t)$, is directly measured by X-ray Photon Correlation Spectroscopy (XPCS) and neutron spin echo. We further calculate the Fourier transformation of $F(Q,t)$ over the momentum transfer Q, as the total scattering is converted into the PDF. This provides the real-space dynamics described by the Van Hove correlation function, $G(r,t)$.

Van Hove Correlation Function is given by:

$$G(R,t) = \frac{1}{4\pi\rho NR^2}\sum_{i,j}\delta\left(R - \left|\boldsymbol{r}_i(0) - \boldsymbol{r}_j(t)\right|\right)$$

Here, ρ is the average particle number density, N is the number of particles, $\boldsymbol{r}_i(t)$ is the position of ith particle at time, t. $\delta(R)$ is Dirac's delta function. Van Hove Correlation function is divided into the self-part $G_s(r,t)$ and the distinct-part $G_d(r,t)$. When X-rays are used, we usually observe coherent scattering except the Compton scattering[2]. Thus, the Van Hove correlation function obtained from X-ray scattering is $G = G_s + G_d$. If we measure only the incoherent scattering as in incoherent neutron scattering, the Van Hove correlation function corresponds to the self part, $G_s(r,t)$. At $t \to 0$, $G_d(r,t)$ is identical to the PDF and $G_s(r,t)$ becomes the Delta function, $\delta(r)$.

2.2. Conversion from reciprocal-space/energy space to real-space/time

To convert $S(Q,E)$ or $F(Q,t)$ into $G(R,t)$, we need to calculate their Fourier transformation. Ideally, the Fourier transformation needs to be carried out over infinite space. In a real world, the measurable E-range and Q-range are finite, which involves the truncation effect associated with the Fourier transform in finite space. To mitigate this effect, we need to measure the spectra over Q and E as wide as possible. When there are points where the spectra show discontinuity, particularly when the spectra at the upper limit of energy transfer $E_{\max}$ and momentum transfer, $Q_{\max}$ are not zero, then the effect of discretization becomes manifest in the transformed spectra. When the intra-molecular motion and high-energy excitation can be ignored, the spectra become a decreasing function. Then if the time-scale of system is within the time-window of instrument, the Fourier transformation over energy transfer hardly suffers from the truncation errors. On the other hand, the Fourier transformation over Q is always affected by the truncation errors as described below. An example of IXS experiment of water at SPring-8 BL43LXU [23-25] is shown in **Fig. 2**. The energy of X-ray was 21.747 keV and the spectra were recorded in $0.94 < Q < 10.1$ Å^{-1} and $-10 < E < 100$ meV. In the case of PDF measurement, using high-energy X-rays can extend the upper limit of Q. The same approach is not feasible in IXS because of the limitation on X-ray energy and the maximum angle that can be measured and currently $Q_{\max}$ is limited to around 10 Å^{-1}. So, we first calculated the Fourier transformation over energy and obtained $F(Q,t)$ (**Fig. 2**). Then, $F(Q,t)$ is Fourier-transformed over Q at each t. Because $F(Q,t=0)$ corresponds to the total scattering intensity, the profile was extrapolated to a

[2] Note that this is different from "scattering of coherent X-rays."

higher Q by using high-energy X-ray scattering intensity that was measured at Advanced Photon Source (Argonne National Laboratory). In this case, we extrapolated the profile up to Q = 20 Å^{-1}. At finite t, the extrapolation procedure is not trivial, but in the case of liquids, the self-diffusive motion is dominant at Q > 10 Å^{-1} and it is reasonable to assume the Gaussian approximation to extrapolate by using $F(Q, t = 0)$. In the current dataset, $F(Q > Q_{\max}, t)$ effectively becomes zero at $t \geq 0.08$ ps and the termination effect associated with the Fourier transformation becomes negligible. Thus, at $t < 0.08$ ps, the termination effect becomes dominant without the extrapolation but at a longer time, the Van Hove correlation function can reliably be estimated.

The time-resolution in the Van Hove function is determined by the energy range used for the Fourier transform. The long-time limit of the Van Hove function is set by the energy resolution of the measurement. Thus, the analyses of liquid dynamics in ps time scales require a high-energy-resolution spectrometer with a meV-resolution. The measured spectra are expressed as the convolution of the true spectra and the energy resolution function. When the IXS spectra are analyzed in the energy domain, model functions convolved with the energy resolution function are used, and the dynamical information, e.g., the width of the dispersion curve, is analyzed. This approach is justified when the model function is obvious but not justified when the choice of model is not evident, particularly for the spectra with weak signals. This issue can be mitigated when the spectrum is converted into the information in the time domain because the convolution in terms of energy can be expressed as the product of intermediate function and the Fourier transform of the energy resolution function in the time domain. The details about the energy resolution function of the spectrometer at BL43LXU, SPring-8, where we have used, are described elsewhere [26]. We used the scattering from borosilicate glass to estimate the energy resolution function.

Because $G(R, t)$ and $S(Q, E)$ are connected via Fourier transform, we often receive the criticism that all the information in $G(R, t)$ is included in $S(Q, E)$ and that there is no new information in $G(R, t)$. But this criticism is not warranted: first, we use *new* information over a wide *Q-E* space that has been ignored in the conventional approaches. Also, the analyses using $S(Q, E)$ highly depends on the model which we choose. There is also a misunderstanding that the real-space correlation at $R = \Delta R$ corresponds to the reciprocal-space correlation at $Q = 2\pi/\Delta R$. It is not straightforward to discuss the molecular dynamics just looking at $S(Q, E)$ as clearly shown in **Fig. 2** but it is obvious that $G(R, t)$ shows the correlation between neighboring molecules. In liquid, the real-space description using $G(R, t)$ is a powerful approach in the same way that the PDF analyses have been useful for carrying out the local structural study of non-crystalline as well as crystalline materials.

3. Examples

3.1. Real-space dynamics in water and aqueous salt solution

The real-space analysis using the Van Hove correlation functions is used for water [16,17] and aqueous salt solution [27,28]. The Van Hove correlation function of pure water is shown in **Fig. 2**. These spectra correspond to oxygen–oxygen correlation because the scattering from hydrogen is negligible compared to that from oxygen in the case of X-rays. At the first neighbor (2.8 Å), the position of the correlation peak moves toward a large *R*, while at the second neighbor (4.5 Å) moves toward the opposite direction. This peak shift indicates that the dynamics at the first and second neighbors are not independent but are dynamically correlated. Such a correlated shift in the peak position is also observed in molecular dynamics simulation using various kinds of water potential but not in metallic liquid [16].

At the first neighbor, the peak intensity shows a two-step decaying behavior, as shown in **Fig. 3**. The first-step decay does not depend on temperature at room temperature, and we speculate that this relaxation corresponds to the rattling-like motion inside a cage made of the surrounding molecules. The second step decay depends on temperature and its decaying time was found to be comparable to τ_{LC} that is defined by the time to lose one neighbor by examining the result of molecular dynamics simulation. For liquid metals at $T > T_A$, where T_A is the viscosity crossover temperature, there is a relationship $\tau_M \sim \tau_{LC}$ where τ_M is the Maxwell relaxation time $\tau_M = \eta/G_\infty$ [29]. Our result shows that water shows a similar relationship, indicating the existence of universality that the macroscopic timescale characterizing viscosity and microscopic timescale characterizing the configurational changes among molecules.

The above discussion applied to the system where only one component, water, exists in the system and the intra-molecular motion was also ignored. When there are more than two components in a system or the intra-molecular motion cannot be ignored, the measured spectra become complicated accordingly. To describe the dynamics in such a system, e.g., an aqueous salt solution, we have introduced the pseudo-partial Van Hove correlation function, which is similar to the partial correlation function used in the structural analysis of a multi-component system [28]. For example, the Van Hove correlation function of low-concentration aqueous salt solution is approximated as follows:

$$G(R,t) - 1 \approx \overline{w_{\mathrm{WW}}}[G_{\mathrm{WW}}{}'(R,t) - 1] + \overline{w_{\mathrm{WC}}}[G_{\mathrm{WC}}{}'(R,t) - 1] + \overline{w_{\mathrm{WA}}}[G_{\mathrm{WA}}{}'(R,t) - 1]$$

Here W, C, A represent water, cation, and anion, respectively. We assume that the correlation between anion and cations can be ignored at a short distance. $\overline{w_{\alpha\beta}}$ is the weighting coefficient that was introduced by Warren and is defined as follows when the scattering is measured at $Q < Q_{\max}$:

$$\overline{w_{\alpha\beta}} = \frac{1}{Q_{\max}} \int_0^{Q_{\max}} w_{\alpha\beta}(Q)\, dQ.$$

$$w_{\alpha\beta}(Q) = \frac{c_\alpha c_\beta f_\alpha(Q) f_\beta(Q)}{[\sum_\alpha c_\alpha f_\alpha(Q)]^2}$$

c_α and $f_\alpha(Q)$ are the concentration and atomic form factor of ith element. In the case of neutron scattering, the Q-dependence of atomic form factor can be ignored, but not in the case of X-ray scattering. So, the averaged weighting factor, $\overline{w_{\alpha\beta}}$, was used. As summarized in Ref. [27] for $w_{\alpha\beta}(Q)$ of NaCl aqueous solution, $\overline{w_{\alpha\beta}}$ of ionic correlation is significantly small and it is reasonable to approximate the Van Hove correlation function using the above three terms. **Fig. 4** shows the pseudo-Van Hove partial correlation functions of the aqueous solution of NaCl, NaBr, and NaI (molality: 1.5 mol/kg). At short times, there exist the termination effect associated with the Fourier transformation, but two positive correlation peaks and one negative correlation peak are clearly observed. The positive correlation peaks appear at $R = R_{\mathrm{O}^{2-}} + R_{\mathrm{C}}$ と $R = R_{\mathrm{O}^{2-}} + R_{\mathrm{A}}$ で where $R_{\mathrm{O}^{2-}}$, R_{C}, and R_{A} are the ionic radius of O^{2-}, cation, and anion, respectively. The negative correlation peak appears at $R = 2R_{\mathrm{O}^{2-}}$. Analyzing the relaxation behavior at this position enables us to study the dynamics between neighboring molecules/ions in aqueous salt solution. In this way, correlation function in terms of both time and distance makes it possible to disentangle the correlation in multi-component system.

Real-space analyses using the Van Hove correlation function can be combined with the molecular dynamics simulation to discuss the detailed motion of each molecule. This approach can also be used as a benchmark for evaluating the potential that is used in the simulation. There are many models of water

potential. Several benchmarks are used for the water potential, such as density, specific heat, and the PDF determined by X-ray and neutron scattering is one of the atomic-scale benchmarks. However, the PDF represents just the averaged snapshot and does not reflect the dynamic nature of liquids. We compared the Van Hove correlation functions determined by various classical MD and ab-initio MD and showed that the experimental Van Hove correlation function could be the benchmark that reflects the dynamic nature of liquids [30].

3.2. Analyses of self-motion using Van Hove correlation function

When discussing the dynamics of liquids at atomic or molecular scales, the self-diffusive motion is often studied. Tracer measurement and field gradient nuclear magnetic resonance (NMR) have been widely used to measure the self-diffusive motion in liquid. Their spatial resolution is far greater than the length scale of atomic-level dynamics and the self-diffusion dynamics determined by these methods are macroscopic. Quasi-elastic incoherent neutron scattering and dynamic light scattering measurements provide information about the self-diffusive dynamics via $S(Q,E)$ and $F(Q,t)$. These techniques can probe the dynamics in a length scale much smaller than that in tracer and NMR. For simple liquids, these different techniques provide essentially the same result regardless of the different length scales being measured [20].

In quasi-elastic neutron scattering, the self-diffusive dynamics is analyzed by using the data taken at Q < 1–3 Å^{-1}. This Q-range corresponds to the length scale after the multiple collisions. The local dynamics before or at the onset of diffusion can be inferred by fitting low-Q spectra using a model such as the jump-diffusion model [31]. However, the details of the atomic-level dynamics remain unexplored at a timescale for the onset of diffusion, which bridges the short-time vibrations and the long-time hydrodynamic diffusive behavior.

We thus studied the self-motion of water by using the Van Hove correlation function [32]. As shown in **Fig. 5**, the Van Hove correlation function at around $r = 0$ is described by the Gauss function (Gaussian approximation):

$$G_s(R,t) = \frac{C(t)}{\rho}\left[\frac{1}{\pi\alpha(t)}\right]^{\frac{3}{2}} e^{-R^2/\alpha(t)}$$

Here the hydrodynamic diffusive behavior is described by $\alpha(t) = 4Dt$ and ideal gas-like behavior is described by $\alpha(t) = \frac{2k_BTt^2}{m}$ [21]. The coefficient $C(t)$ is introduced to take account the difference from the Gaussian approximation. By calculating the mean squared displacement $\langle r^2(t)\rangle = \frac{3\alpha(t)}{2}$, we obtained $\langle r^2(t)\rangle \sim t$ at t > 0.4 ps. The self-diffusion coefficient D_{VHF} that was calculated by using the data at t > 0.6 ps is compared with macroscopic self-diffusion coefficient D_{Macro} in **Fig. 6**. As the temperature lowers, the discrepancy between D_{VHF} and D_{Macro} becomes larger. We suspect that this discrepancy reflects the difference of length-scale that is described by these quantities: D_{Macro} corresponds to the diffusive behavior at hydrodynamic limit, while D_{VHF} observes local self-dynamics at $\langle r^2(t)\rangle < 2$ Å^2. Conventional approach using incoherent neutron scattering at low-Q measures the dynamic corresponding to the length scale where the multiple collisions take place and has not provided the information of the onset of diffusion process. Our results demonstrate that the self-part of the Van Hove correlation function can be determined by experiment with the high-resolution inelastic X-ray scattering over momentum transfer wide enough to mitigate the termination effect. The same approach can be utilized for other liquids using both inelastic X-ray and neutron scattering.

3.3. Analyses of pico-second dynamics using X-ray Free Electron Laser

The real-space approach using the Van Hove correlation function enables us to visualize the local dynamics in liquid. Water dynamics happens to be within the time window of high-resolution IXS at SPring-8, but access to much slower dynamics is needed to study supercooled water and other liquids. Backscattering of neutron and neutron spin echo spectroscopy provide the relevant energy resolution, but their Q-range is usually restricted to the narrow range, which prevents us from transforming the spectra into real-space information. To expand the real-space approach to much slower dynamics, we used X-ray Photon Correlation Spectroscopy (XPCS) using an X-ray Free Electron Laser (XFEL).

Analyses of dynamics in liquid using XPCS with XFEL have been proposed since the project of XFEL was initiated [33,34]. In conventional XPCS, coherent X-rays are used, and the temporal correlation of speckled scattering images provides the intermediate scattering function. The temporal resolution is set by the temporal resolution of the detector (in SR) or the repetition rate of XFEL (in XFEL), making it difficult to measure the dynamics in picoseconds and nanoseconds. When scattering at a large scattering angle is measured, the path difference of scattering can be longer than the temporal coherence length depending on the beam size and sample size. In this case, the speckle is not observed, impeding the measurement of atomic-scale dynamics. The limitation is mitigated by using two X-ray pulses generated from a single XFEL pulse. The X-ray pulses are separated in time, and the sum of speckle scattering patterns from a sequence of two separate X-ray pulses is analyzed. This approach uses the concept of Speckle Visibility Spectroscopy (SVS) [35-39] that was developed using a visible light laser. The accessible timescale is determined by the time separation between the two pulses, making it possible to study the dynamics in femtoseconds, picoseconds, and sub-nanoseconds. A similar approach with variable pulse duration has recently been demonstrated for the femtoseconds dynamics in supercooled water [40]. The key component to realizing this approach is Split-Delay Optics (SDO), which creates two sub-pulses from a single XFEL pulse and controls a delay time between the sub-pulses by their path length difference [41,42]. An SDO system for the XPCS has been developed, and a few experimental results at small-angle scattering range where the experimental difficulty is rather low has been reported [43]. However, the study of atomic-level dynamics at a sub-nm scale with an SDO has not been reported because of the lack of SDO stability and the insufficient pulse energy of X-rays.

To improve the statistics, we used the highly stable SDO [41] developed at SACLA [44] and a seeded XFEL[45] [46]. Room-temperature water was measured at BL3, SACLA. The experimental layout is shown in **Fig. 7**. By using an SDO at the optical hutch, the time-delay of 0-2 ps between two-pulses was created and the two pulses were focused on the sample position with 0.7 μm (H) x 0.9 μm using an X-ray mirror. The sample was water jet stream with the radius of 25 μm. The X-ray energy was 10 keV. The scattering images were recorded by several MPCCD which located at 1 m downstream of the sample. A typical scattering image from the sample shown in **Fig. 8** shows that the number of measured photons is small. This makes it difficult to calculate the contrast of speckle images directly. To mitigate this difficulty, the visibility was calculated by the maximum likelihood of the statistics of observed photons by assuming that the probability for observing k photons at a single pixel is described by a negative binomial distribution [39,40,43,47]. This approach can be used only if the frequency of measuring more than two photons at a single pixel is not too small. When a conventional SASE XFEL is used, the averaged single-shot X-ray energy at sample position is 0.38 μJ and it is not possible to record data when the water jet of 25 μm is used.

The use of seeded XFEL makes it possible to use 7.7 μJ of X-ray pulse on average, which allows us to measure multiple photons at several pixels.

Fig. 9 shows the speckle contrast that is estimated by the maximum likelihood. I_{fixed} is the pulse energy of the first pulse. The dependence of the contrast on Δt agrees with the intermediate scattering function that is calculated from the IXS measurement. At $I_{\mathrm{fixed}} > 3\ \mu$J, there are discrepancies in this Q-range due to the heating effect by the first X-ray pulse [46,48]. Measurement at XFEL records various quantities and parameters shot-by-shot, which makes it possible to post-process the data to extract the reliable experimental data that are hardly influenced by the heating and other unwanted effect.

As highlighted in the fact that one of the first beamlines at LCLS was X-ray Correlation Spectroscopy [49], the measurement of atomic-scale dynamics using the SDO has been explored at each XFEL facility in the world. Our measurement is the first successful measurement of atomic-scale dynamics with controlling the picosecond-scale time-delay using the SDO. This success at SACLA is the result of highly brilliant seeded XFEL and the high stability of X-ray optics available at SACLA. In particular, the SDO at SACLA is notable for its long-time stability, as exemplified in [46]. Future studies at wider Q and time-delay would determine the Van Hove correlation function at a timescale that is hard to measure using the IXS.

4. Perspective

This review discusses the real-space approach to studying the liquid dynamics, particularly water and aqueous salt solution, using the Van Hove correlation function obtained from X-ray scattering. The key to this approach is a careful measurement of spectra that have been thought useless and discarded. The current approach can be used for not only liquids but other systems such as a highly disordered system where the reciprocal space description is not appropriate. Combining X-ray and neutron scattering will enable us to change the scattering contrast, leading to detailed analyses of dynamics as has been done for structural analyses using PDF. Furthermore, other scattering contrast such as magnetic scattering can also be converted into the real-space correlation function, which will make it possible to extract the real-space correlation that is otherwise hidden in reciprocal space.

Decades ago, it was a dream for many researchers to measure the dynamic structure factor over wide *Q-E* and to determine the Van Hove correlation function of liquid [50]. Thanks to recent progress in X-ray and neutron scattering techniques, such a dream comes true. We hope this review helps study the dynamics of liquids hidden in reciprocal space.

References

[1] H. D. B. Jenkins and Y. Marcus, Chemical Reviews **95**, 2695 (1995).
[2] G. Jones and M. Dole, Journal of the American Chemical Society **51**, 2950 (1929).
[3] Y. Marcus, Chemical Reviews **109**, 1346 (2009).
[4] T. Egami and S. J. L. Billinge, *Underneath the Bragg Peaks: Structural Analysis of Complex Materials* (Elsevier, Amsterdam, 2012), 2nd edn.
[5] R. Mancinelli, A. Botti, F. Bruni, M. A. Ricci, and A. K. Soper, The Journal of Physical Chemistry B **111**, 13570 (2007).
[6] H. J. Bakker, Chemical Reviews **108**, 1456 (2008).
[7] Y. Chen *et al.*, Science Advances **2**, e1501891 (2016).
[8] F. Perakis, L. De Marco, A. Shalit, F. Tang, Z. R. Kann, T. D. Kühne, R. Torre, M. Bonn, and Y. Nagata, Chemical Reviews **116**, 7590 (2016).
[9] A. Shalit, S. Ahmed, J. Savolainen, and P. Hamm, Nature Chemistry **9**, 273 (2017).

[10] Y. Yamada, J. Wang, S. Ko, E. Watanabe, and A. Yamada, Nature Energy (2019).
[11] U. Balucani and M. Zoppi, *Dynamics of the Liquid State* (Oxford University Press, New York, 1994), Oxford Series on Neutron Scattering in Condended Matter.
[12] G. Monaco, A. Cunsolo, G. Ruocco, and F. Sette, Physical Review E **60**, 5505 (1999).
[13] L. Van Hove, Physical Review **95**, 249 (1954).
[14] R. Ashcraft, Z. Wang, D. L. Abernathy, D. G. Quirinale, T. Egami, and K. F. Kelton, The Journal of Chemical Physics **152**, 074506 (2020).
[15] T. Egami, Frontiers in Physics **8**, 50 (2020).
[16] T. Iwashita, B. Wu, W.-R. Chen, S. Tsutsui, A. Q. R. Baron, and T. Egami, Science Advances **3**, e1603079 (2017).
[17] Y. Shinohara, W. Dmowski, T. Iwashita, B. Wu, D. Ishikawa, A. Q. R. Baron, and T. Egami, Physical Review E **98**, 022604 (2018).
[18] B. N. Brockhouse and N. K. Pope, Physical Review Letters **3**, 259 (1959).
[19] J. P. Boon and S. Yip, *Molecular Hydrodynamics* (McGraw-Hill, New York, 1980).
[20] P. A. Egelstaff, *An Introduction to the Liquid State* (Oxford University Press, New York, 1992).
[21] J.-P. Hansen and I. R. McDonald, *Theory of Simplie Liquids: with Applications to Soft Matter* (Academic Press, New York, 2013).
[22] U. Dahlborg, W. Gudowski, and M. Davidovic, Journal of Physics: Condensed Matter **1**, 6173 (1989).
[23] A. Q. R. Baron, in *Synchrotron Light Sources and Free-Electron Lasers*, edited by E. J. Jaeschke *et al.* (Springer International Publishing, Cham, 2016), pp. 1643.
[24] A. Q. R. Baron, in *Synchrotron Light Sources and Free-Electron Lasers*, edited by E. Jaeschke *et al.* (Springer International Publishing, Cham, 2016), pp. 1721.
[25] A. Q. R. Baron, SPring-8 Information Newsletter **15**, 14 (2010).
[26] D. Ishikawa and A. Q. R. Baron, Journal of Synchrotron Radiation **28**, 804 (2021).
[27] Y. Shinohara, W. Dmowski, T. Iwashita, D. Ishikawa, A. Q. R. Baron, and T. Egami, Physical Review Materials **3**, 065604 (2019).
[28] Y. Shinohara *et al.*, The Journal of Physical Chemistry Letters **10**, 7119 (2019).
[29] T. Iwashita, D. M. Nicholson, and T. Egami, Physical Review Letters **110**, 205504 (2013).
[30] R. A. Matsumoto *et al.*, J Chem Theory Comput **17**, 5992 (2021).
[31] C. T. Chudley and R. J. Elliott, Proceedings of the Physical Society **77**, 353 (1961).
[32] Y. Shinohara, W. Dmowski, T. Iwashita, D. Ishikawa, A. Q. R. Baron, and T. Egami, Physical Review E **102**, 032604 (2020).
[33] G. Grübel, G. B. Stephenson, C. Gutt, H. Sinn, and T. Tschentscher, Nuclear Instruments and Methods in Physics Research Section B: Beam Interactions with Materials and Atoms **262**, 357 (2007).
[34] G. B. Stephenson, A. Robert, and G. Grübel, Nature Materials **8**, 702 (2009).
[35] R. Bandyopadhyay, A. S. Gittings, S. S. Suh, P. K. Dixon, and D. J. Durian, Review of Scientific Instruments **76**, 093110 (2005).
[36] P. K. Dixon and D. J. Durian, Physical Review Letters **90**, 184302 (2003).
[37] I. Inoue, Y. Shinohara, A. Watanabe, and Y. Amemiya, Optics Express **20**, 26878 (2012).
[38] Y. Sun, J. Montana-Lopez, P. Fuoss, M. Sutton, and D. Zhu, Journal of Synchrotron Radiation **27**, 999 (2020).
[39] J. Verwohlt, M. Reiser, L. Randolph, A. Matic, L. A. Medina, A. Madsen, M. Sprung, A. Zozulya, and C. Gutt, Physical Review Letters **120**, 168001 (2018).
[40] F. Perakis *et al.*, Nature Communications **9**, 1917 (2018).
[41] T. Hirano *et al.*, Journal of Synchrotron Radiation **25**, 20 (2018).
[42] T. Osaka, T. Hirano, Y. Sano, Y. Inubushi, S. Matsuyama, K. Tono, T. Ishikawa, K. Yamauchi, and M. Yabashi, Optics Express **24**, 9187 (2016).
[43] W. Roseker *et al.*, Nature Communications **9**, 1704 (2018).
[44] T. Ishikawa *et al.*, Nature Photonics **6**, 540 (2012).
[45] I. Inoue *et al.*, Nature Photonics **13**, 319 (2019).

[46] Y. Shinohara, T. Osaka, I. Inoue, T. Iwashita, W. Dmowski, C. W. Ryu, Y. Sarathchandran, and T. Egami, Nature Communications **11**, 6213 (2020).
[47] S. O. Hruszkewycz *et al.*, Physical Review Letters **109**, 185502 (2012).
[48] E. Zarkadoula, Y. Shinohara, and T. Egami.
[49] R. Alonso-Mori *et al.*, J Synchrotron Radiat **22**, 508 (2015).
[50] 三沢正勝, 日本中性子学会誌「波紋」 **18**, 108 (2008).
[51] M. Holz, S. R. Heil, and A. Sacco, Physical Chemistry Chemical Physics **2**, 4740 (2000).

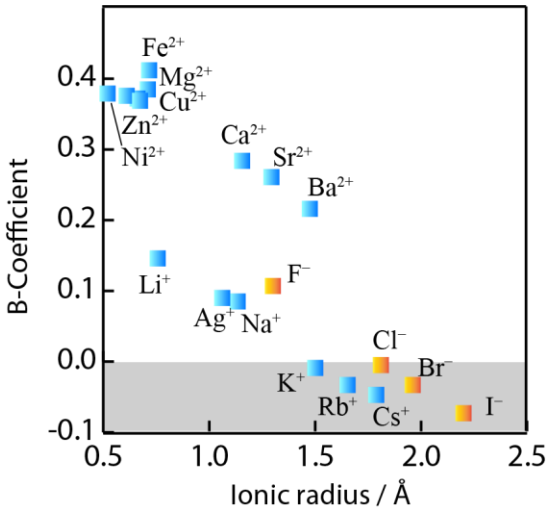

Fig. 1 (Color online) Viscosity B-coefficient at room temperature. Data taken from Ref. [1].

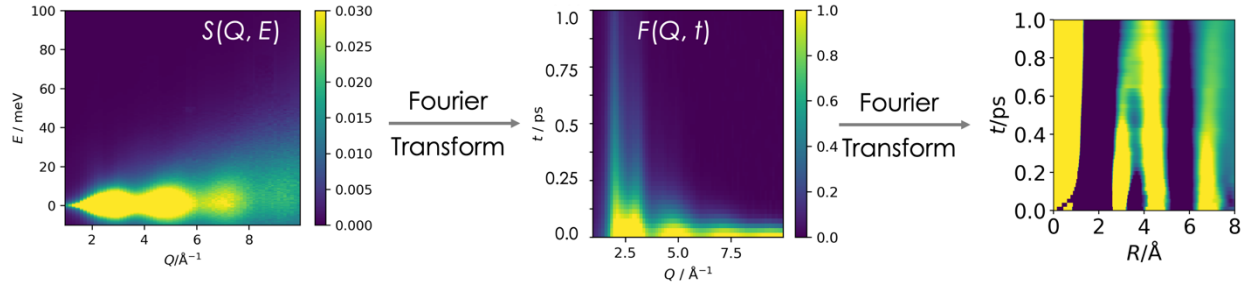

Fig. 2 Dynamic structure factor, $S(Q, E)$, intermediate scattering function, $F(Q, t)$, and the Van Hove correlation function, $G(R, t)$, of pure water at room temperature.

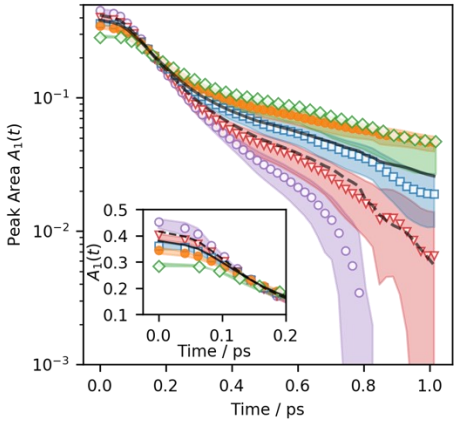

Fig. 3: Temporal changes in the area of the first-neighbor neighbor correlation in aqueous solution of sodium chloride and their enlarged view (inset): (open circles) pure water, (triangles) m = 0.75 mol/kg,

(squares) 1.5 mol/kg, (closed circles) 2.26 mol/kg, and (diamonds) 3.0 mol/kg. The shaded areas represent uncertainties of each dataset. Figures are taken from [27].

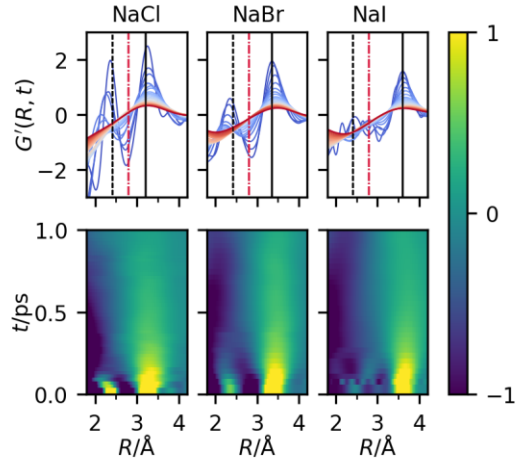

Fig. 4: Pseudo-partial Van Hove Correlation Function of aqueous solution of NaCl, NaBr, and NaI (m = 1.5 mol/kg). Figures are taken from [28].

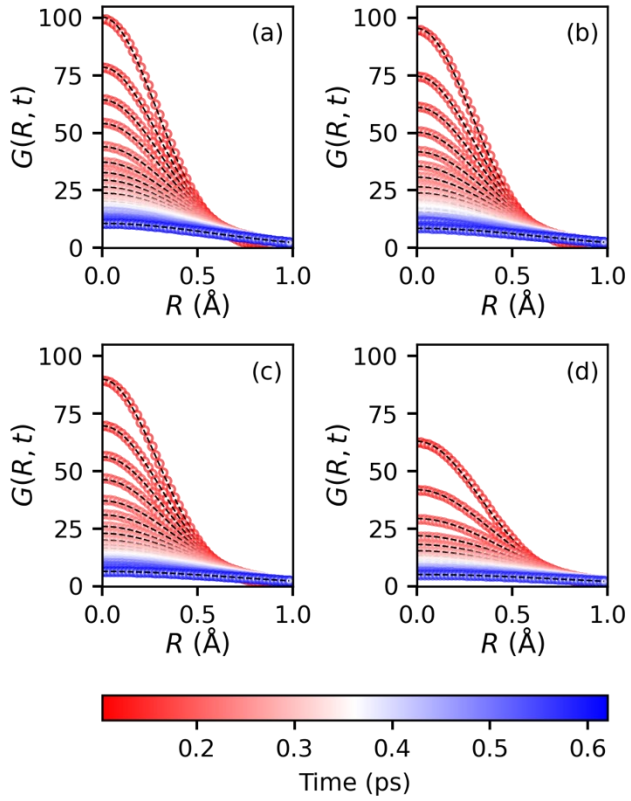

Fig. 5: Self-part of the Van Hove correlation function of water at (a) 285 K, (b) 295 K, (c) 310 K, and (d) 318 K. The symbols represent the experimental data, and the dashed lines represent the fitting results using the Gaussian approximation. Figures are taken from [32].

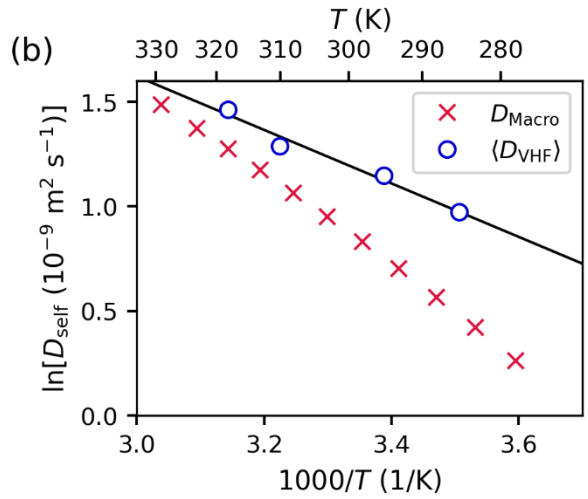

Fig. 6: Self-diffusion coefficients extracted from the IXS experiment (D_{VHF}) and from a reference (D_{Macro})[51]. Figures are taken from [32].

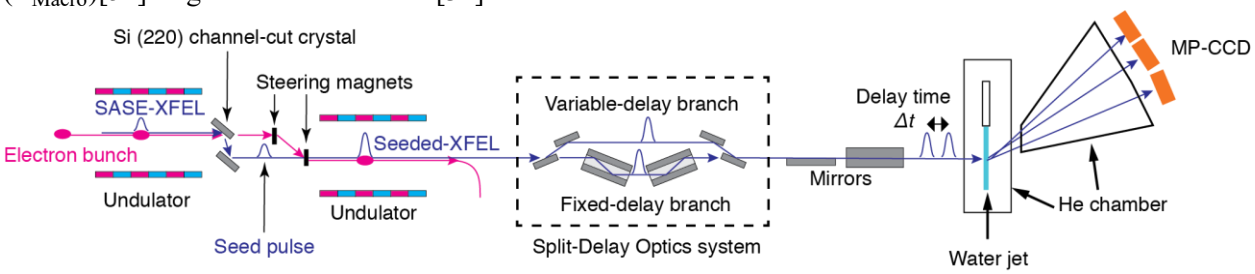

Fig. 7: Setting of the XSVS using XFEL at SACLA BL3. The seed pulse was produced by monochromatizing the SASE from the upstream undulator segments. Then the seed was amplified in the downstream undulation. The amplified X-ray pulse was split into two sub-pulses using the SDO. The sub-pulses with a delay time are focused by mirrors and hit the water jet. Scattered X-rays were recorded by the MPCCDs. Figure taken from Ref. [46].

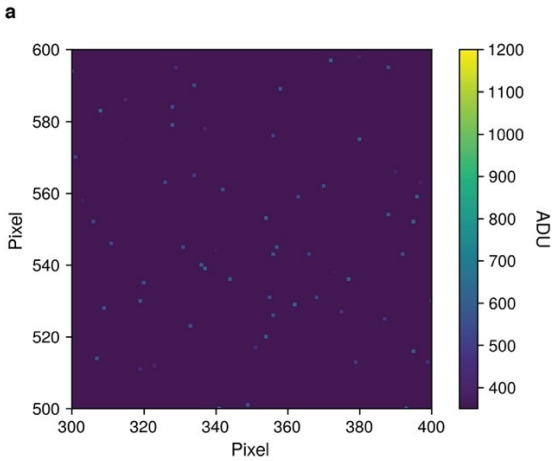

Fig. 8: Example of single-shot scattering image from water at around Q = 2 Å^{-1}. Single photon energy of 10 keV X-ray corresponds to ~ 590 ADU. Figure taken from Ref. [46].

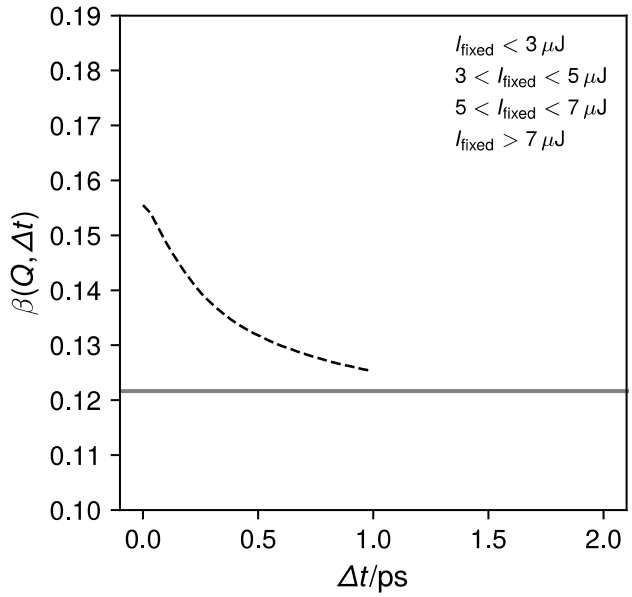

Fig. 9: Comparison of XSVS result and IXS results at $Q = 2.00 \pm 0.06$ Å^{-1}. The solid line represents the contrast measured when there was no overlap between two sub-pulses. The uncertainty was calculated using the second derivative of the log-likelihood. The dashed lin represents the decaying behavior that is estimated by the result of IXS. Figure taken from Ref. [46].

Acknowledgement

This work was supported by the U. S. Department of Energy, Office of Science, Office of Basic Energy Science, Division of Materials Sciences and Engineering. The IXS experiments at SPring-8 BL43LXU were carried out under the approval of RIKEN (Proposal No. 20170075, 20180069, 20190002). The X-ray experiments at BL3, SACLA were carried out under the approval of JASRI (Proposal No. 2018B8041, 2019A8043, 2019B8011). IXS experiment at SPring-8 BL43LXU was collaborated with Dr. Alfred Q. R. Baron and Dr. Daisuke Ishikawa. MD simulation of aqueous salt solution was collaborated with Prof. P. Cummings, Dr. M. W. Thompson, and Dr. R. Matsumoto. Simulation of Van Hove Correlation function was collaborated with Dr. P. C. R. Kent, S. Irle, and Prof. A. C. T. van Duin. The X-ray experiment at SACLA was supported by Dr. T. Osaka and I. Inoue. The X-ray scattering experiments were carried out with the collaboration with Drs. C. W. Ryu, W. Dmowski (University of Tennessee).